Pergamon

Int. J. Heat Mass Transfer. Vol. 39, No. 5, pp. 995–1004, 1996

0017-9310/96 $15.00 + 0.00

0017-9310(95)00187-5

Numerical simulation of the transient moisture transfer through porous insulation

N. E. WIJEYSUNDERA,† B. F. ZHENG, M. IQBAL‡ and E. G. HAUPTMANN

Department of Mechanical Engineering, University of British Columbia, Vancouver, B.C., Canada V6T 1Z4

(*Received* 5 *May* 1994 *and in final form* 13 *May* 1995)

Abstract—This paper develops a numerical model for simulating heat and moisture transfer through a porous insulation, with impermeable, adiabatic vertical boundaries, and with one horizontal boundary facing a warm humid ambient and the other facing a cold impermeable surface. The problem is modeled as one-dimensional, transient, multi phase flow with variable physical properties. The analysis has identified four phases of energy and moisture transport processes, and they are formulated by a system of transient intercoupled equations and several thermodynamic relations using the local volume averaging technique. The numerical model is validated by comparing with experimental data for different operating conditions and for times up to 600 h. The model predicts the temperature distribution, the heat transfer and the total moisture gain successfully. The predicted liquid distribution agrees with measured data for a period of up to 70 h. The interesting effects of pertinent parameters on the energy and moisture transfer in the porous insulation are investigated.

INTRODUCTION

The simultaneous flow of heat and moisture in building materials has received considerable attention in the recent literature. Moisture transport results in condensation–evaporation processes which accompany energy transfer through building envelopes. The moisture ingress into building components, particularly porous thermal insulation over a long period will lead to the accumulation of water, which in turn results in the corrosion of the insulated metallic components of the system.

Ideally, the use of a vapor barrier on the warm side of a porous building component should prevent the ingress of water vapor. However, in actual practice this is not completely realized due to difficulties with installation and cracks that develop with time. From a design stand point it is useful to understand and quantify these heat and mass transfer processes. Such an understanding may lead to methods of preventive maintenance which will enable us to drive moisture out and dry insulations to re-establish its effectiveness.

Investigations of heat and moisture transport in insulation may be classified as (a) laboratory studies, (b) field studies and (c) analytical–numerical design studies. Although very useful, laboratory and field studies are time consuming because in practical situations, moisture transfer occurs slowly. Also it is difficult to cover a wide range of operating and design conditions in such work. Laboratory work was reported by Kumaran [1, 2], Wijeysundera *et al.* [3, 4], and Modi and Benner [5, 6]. Extensive field investigations have ben carried out by Heldin [7].

Analytical studies on moisture and heat transfer were reported by Ogniewicz and Tien [8], Motakef and El-Masri [9] and Shapiro and Motakef [10]. These papers mainly dealt with the quasi-steady phase of the transfer processes. Vafai and co-workers [11–14] have performed extensive numerical simulations of heat and moisture transfer processes in porous insulations. They have used both one-dimensional (1D) and two-dimensional (2D) models to predict the heat transfer parameters. Tao *et al.* [15] have used numerical simulations to study frosting effects in fibrous insulations.

The experimental results reported by Wijeysundera *et al.* [3, 4] showed the variation of a few physical parameters during the short-term and long-term moisture transfer in an insulation slab. Based on these measurements suggestions were made about the likely physical processes which might be occurring in the insulation. The aim of the present study is to perform a detailed numerical simulation to verify the existence of the different phases of the moisture transfer process and there by interpret physically the experimental measurements. Also, the effect of the transient variation of physical properties such as the thermal conductivity, the vapor and liquid diffusivity due to liquid accumulation on the dynamic behavior of the insulation is investigated in the present study.

In the next section the governing equations and the numerical procedure are outlined. The subsequent sections give the numerical results, comparisons and discussions.

† On sabbatical leave from National University of Singapore.

‡ Author to whom correspondence should be addressed.

NOMENCLATURE

B	heat transfer Biot number, $h\,L/k^*$
B_m	mass transfer Biot number, $h_m L/D_v^*$
c_p	nondimensional specific heat capacity, c_p^*/c_{p0}^*
D_v	nondimensional vapor diffusivity, D_v^*/α_{e0}^*
D_l	nondimensional liquid diffusivity, D_l^*/α_{e0}^*
D_{12}	binary diffusion coefficient [m^2 s^{-1}]
Fo	Fourier number, $t^*\alpha_{e0}/L^2$
g	Clausius–Clapeyron relation, ρ_v^*/ρ_0^*
G	nondimensional condensation rate, $\Gamma L^2/\rho_0^*\alpha_{e0}^*$
h	ambient heat transfer coefficient [W m^{-2} K^{-1}]
h_m	ambient mass transfer coefficient [kg m^{-2} s^{-1}]
h_{fg}	specific enthalpy of phase change [J kg^{-1}]
k	nondimensional thermal conductivity, k^*/k_0^*
k_{dry}	dry thermal conductivity [W mK^{-1}]
k_{eq}	equivalent thermal conductivity [W m K^{-1}]
k_{eff}	effective thermal conductivity of slab [W m K^{-1}]
K	nondimensional hydraulic conductivity, K^*L/α_{e0}
L	thickness of slab [m]
p_i	nondimensional pressure, p_i^*/p_{v0}^*
p_{total}	nondimensional total gas pressure
P_1	nondimensional parameter, ρ_β^*/ρ_0^*
P_2	nondimensional parameter, $h_{fg}/\Delta T c_{p0}^*$
P_3	nondimensional parameter, $\Delta T R_v \rho_0^*/p_{v0}^*$
P_4	nondimensional parameter, $\Delta T R_a \rho_0^*/p_{v0}^*$
P_5	nondimensional parameter, $h_{fg}/\Delta T R_v$
q_i	total heat flux in slab [W m^{-2}]
q_2	total heat flux at cold surface [W m^{-2}]
R	gas constant [J kg^{-1} K^{-1}]
RH	ambient relative humidity [%]
S	liquid saturation
T	temperature of slab [K]
T_0	reference temperature in equation (13) [K]
T_a	ambient temperature [K]
T_2	temperature of cold surface [K]
t	nondimensional time, $t^*\alpha_{e0}/L^2$
w	weight liquid content
x	distance along slab [m]
z	nondimensional distance, x/L.

Greek symbols

α_{e0}^*	effective thermal diffusivity, $k_0^*/\rho_0^* c_{p0}^*$
ΔT	temperature difference, $(T_a - T_2)$
ε	volume fraction
ε_0	void fraction of dry slab
ε_v	void fraction of slab with liquid
Γ	condensation rate per unit volume [kg m^{-3} s^{-1}]
ρ_i	density [kg m^{-3}]
τ	tortuosity factor
θ	nondimensional temperature, $T/\Delta T$.

Subscripts

ai	air
a	ambient
d	dry state
l	liquid
v	vapor phase
γ	gas phase
σ	solid phase
β	liquid phase
0	reference condition.

Superscripts

*	dimensional quantity.

PHYSICAL MODEL

The physical system is modeled as a porous slab with impermeable and adiabatic vertical boundaries as shown in Fig. 1(a). The upper horizontal boundary is impermeable and subjected to a cold temperature, and the lower one is exposed to an ambient that is warm and humid. Initially, the slab is assumed to be fully dry with a uniform temperature equal to the ambient temperature and the vapor density equal to the ambient vapor density. It is suddenly subjected to a temperature drop at the upper impermeable surface.

The water vapor will migrate into the insulation due to the vapor density gradient and the temperature gradient, and it is expected to exhibit four stages of transport processes as shown in Fig. 1.

The first stage is a relatively short initial transient stage in which the temperature and vapor concentration fields are developing within the insulation slab. In the second stage [Fig. 1(b)] the heat and vapor transfer processes reach a quasi-steady state, and the temperature and water vapor density fields are invariable with time. Liquid is accumulated in the wet region, however the liquid content is still low and does not have a significant effect on the transport properties. When liquid accumulation exceeds a critical value, the liquid starts to move due to the generated liquid pressure and will flow towards the wet–dry interface [Fig. 1(c)]. Capillary action could also assist liquid transport. As time proceeds, the liquid front will move into the dry region of the slab. In the last stage, the liquid front eventually reaches the exposed

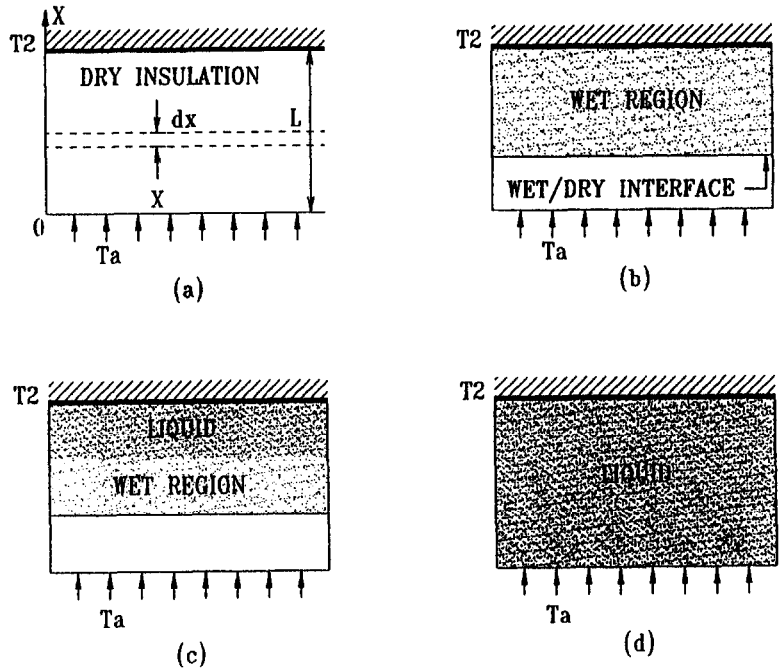

Fig. 1. Schematic of the four stages in the moisture transfer process: (a) initial transient stage, (b) quasi-steady stage, (c) liquid diffusion stage and (d) long-term moisture gain.

surface and liquid accumulation in the slab continues [Fig. 1(d)]. The long-term accumulation of liquid in the insulation is believed to have two important effects: (1) a decrease in the local vapor diffusion coefficient and (2) an increase in the local thermal conductivity of the slab. These factors will both influence the heat transfer and the condensation rate in the slab.

The formulation of this problem is based on the local volume averaging technique [16, 17]. The mass, momentum and energy equations for each phase which make up the governing equations for heat and mass transport in the insulation are derived using the volume averaging method. Several assumptions are made in arriving at the governing equations. (a) The fibrous insulation is homogeneous. (b) The solid–liquid–gas system is in local equilibrium. (c) No convective gas phase flow occurs in the insulation matrix; any moisture accumulation is caused by vapor diffusion only. (d) The total gas pressure in the insulation matrix is constant. (e) For medium density fibrous insulations where the main fiber orientation is horizontal, the effect of gravity on liquid transport can be neglected. Due to assumptions (c) and (d), the gas and liquid pressure distribution can be considered to be hydrostatic.

GOVERNING EQUATIONS

The details of the application of the volume averaging technique to porous insulation systems are available in Vafai *et al.* [11, 12]. The derivation of the governing equations requires considerable algebraic manipulation [16]. The final forms of these governing equations in terms of the nondimensional variables are given as:

Energy equation

$$\frac{\partial}{\partial z}\left[k\frac{\partial\theta}{\partial z}\right]+P_2G=\rho c_p\frac{\partial\theta}{\partial t}. \tag{1}$$

Vapor diffusion equation

$$\frac{\partial}{\partial z}\left[D_v\frac{\partial\rho_v}{\partial z}\right]-G=\frac{\partial(\varepsilon_\gamma\rho_v)}{\partial t}. \tag{2}$$

Liquid transport equation:

The governing equation for liquid transport is formulated in such a manner that measured data on liquid diffusivity could be used. Cid and Crausse [18] measured the liquid diffusion coefficient for fiberglass insulation of different density and fiber size. Their liquid diffusion coefficient $D_l^*(w)$ is defined as in the following liquid transport equation:

$$\frac{\partial w}{\partial t^*}=\frac{\partial}{\partial x}\left[D_l^*(w)\frac{\partial w}{\partial x}+\frac{\rho_\beta^*}{\rho_0^*}K^*(w)\right]+\frac{\Gamma}{\rho_0^*} \tag{3}$$

where w is the mass liquid content, $K^*(w)$ is the hydraulic conductivity and is a function of the liquid saturation S. The relation between w, S and liquid fraction ε_β are

$$w=\frac{\rho_\beta^*}{\rho_0^*}\varepsilon_\beta \tag{4}$$

$$S=\frac{\rho_0^* w}{\rho_\beta^*\varepsilon_0} \tag{5}$$

$$\varepsilon_\beta = \varepsilon_0 S = (1-\varepsilon_\sigma)S \tag{6}$$

where ε_0 is the void fraction of the dry porous insulation.

Equations (4)–(6) are used to transform equation (3) to the form used in the present formulation. In terms of the nondimensional variables, the liquid diffusion equation becomes

$$\frac{\partial \varepsilon_\beta}{\partial t} = \frac{\partial}{\partial z}\left[D_1(\varepsilon_\beta)\frac{\partial \varepsilon_\beta}{\partial z} + K(\varepsilon_\beta)\right] + \frac{G}{P_1}. \tag{7}$$

The liquid diffusion coefficient and hydraulic conductivity in terms of liquid saturation are regressed from Cid and Crausse's experimental data [18]. The following polynomials have less than 5% discrepancy from the original experimental data:

$$\begin{aligned} D_1^*(S) = {} & 1.29\times10^{-8} + 9.913 \\ & \times 10^{-7}S + 1.6018\times10^{-6}S^2 \\ & - 7.8408\times10^{-6}S^3 \\ & + 1.053\times10^{-5}S^4 \\ & (0.45 > S > 0.05) \end{aligned} \tag{8}$$

$$\begin{aligned} K^*(S) = {} & 4.502\times10^{-7} \\ & - 4.658\times10^{-6}S \\ & + 1.05486\times10^{-3}S^2 \\ & - 2.56279\times10^{-3}S^3 \\ & - 1.7555\times10^{-4}S^4 \\ & + 3.956\times10^{-3}S^5. \end{aligned} \tag{9}$$

THE CONSTITUTIVE EQUATIONS

The corresponding constitutive correlations in terms of the nondimensional variables are [11]:
Volumetric constraint;

$$\varepsilon_\sigma + \varepsilon_\beta + \varepsilon_\gamma = 1 \tag{10}$$

Thermodynamic relations;

$$p_v = P_3 \rho_v \theta \tag{11}$$

$$p_{ai} = P_4 \rho_{ai} \theta \tag{12}$$

$$p_v = \exp\left[P_5(1/\theta - 1/\theta_{ref})\right] \tag{13}$$

and

$$p_{total} = p_{ai} + p_v. \tag{14}$$

All the nondimensional variables and the nondimensional parameters P_1–P_5 are defined in the nomenclature.

The spatial average density of the porous insulation is defined as

$$\rho = \varepsilon_\sigma \rho_\sigma + \varepsilon_\beta \rho_\beta + \varepsilon_\gamma \rho_\gamma \tag{15}$$

where

$$\rho_\gamma = \rho_{ai} + \rho_v. \tag{16}$$

The mass fraction weighted average specific heat capacity is defined as

$$c_p = (\varepsilon_\sigma \rho_\sigma c_{p\sigma} + \varepsilon_\beta \rho_\beta c_{p\beta} + \varepsilon_\gamma \rho_\gamma c_{p\gamma})/\rho \tag{17}$$

where

$$c_{p\gamma} = (c_v \rho_v + c_{ai}\rho_{ai})/\rho_\gamma. \tag{18}$$

THERMAL CONDUCTIVITY MODELS

The presence of liquid has a significant effect on the thermal conductivity of the porous insulation. It is believed that the apparent thermal conductivity of moist insulation depends on the manner that the liquid distributes inside the insulation [19].

Three different physical models for liquid distribution in a porous medium are considered in the present study.

(a) *Bead arrangement*

In this model liquid is located as small beads throughout the insulation. The apparent thermal conductivity can be represented by [19]:

$$k^*(\varepsilon_\beta) = k_d^*[1 + 2\varepsilon_\beta Y]/[1 - \varepsilon_\beta Y] \tag{19}$$

where

$$Y = [k_\beta^* - k_d^*]/[k_\beta^* + 2k_d^*]. \tag{20}$$

(b) *Series arrangement*

In this model the liquid is distributed in layers perpendicular to the direction of heat flow. The liquid would then have the maximum in inhibiting the heat flow. For this arrangement,

$$k^*(\varepsilon_\beta) = k_d^* k_\beta^*/[k_\beta^* - X] \tag{21}$$

where

$$X = \varepsilon_\beta(k_\beta^* - k_d^*)/\varepsilon_\gamma. \tag{22}$$

(c) *Parallel arrangement*

In this model the liquid is located in a continuous shape parallel to the direction of heat flow. For this arrangement,

$$k^*(\varepsilon_\beta) = k_d^* + X \tag{23}$$

where

$$X = \varepsilon_\beta(k_\beta^* - k_d^*)/\varepsilon_\gamma. \tag{24}$$

VAPOR DIFFUSIVITY MODEL AND TRANSFER COEFFICIENTS

The vapor–air mixture diffusion coefficient in porous insulation is given by [20]

$$D_v^* = \frac{\varepsilon_v}{\tau} D_{12} \tag{25}$$

where D_{12} is the binary diffusion coefficient of Fick's law; ε_v is the void fraction of the moisture laden slab; τ is the tortuousity. The binary diffusion coefficient for water vapor–air mixture is given by [20]:

$$D_{12} = 1.97 \times 10^{-5}\left[\frac{T}{255.2}\right]^{1.685}. \quad (26)$$

Experimentally estimated values [4] are used for the ambient heat transfer coefficient h and the mass transfer coefficient is obtained by the application of the mass transfer analogy [20].

NUMERICAL SIMULATION

For numerical simulation, the governing equations (1), (2) and (7) are cast in finite difference form using the control volume approach [23]. A fully implicit scheme is chosen for requirements of stability. In general, the central difference form is used for the internal nodes and backward or forward difference is used for boundary nodes. Backward difference form is also used for the time derivative. The details of the numerical formulation are available in ref. [24].

The computation is started by solving the governing equations (1) and (2) for the dry slab. When the local vapour density exceeds the saturation value computed from equation (13), condensation occurs at the node. In the wet region equations (1) and (2) are combined by eliminating G between them. The resulting equation is solved to obtain the temperature distribution which is substituted in equation (1) to obtain G. The solution of equation (7) gives the liquid distribution. When the liquid front passes beyond the condensation wet–dry interface, the wet region is defined by the position of the liquid front.

The grid size and time step size were varied to determine the values that give consistent results for the wet–dry boundary and the field variables. A non-dimensional grid size of 0.001 and a time step of 120 s satisfied both requirements of accuracy and economy of computation. The solution was considered converged when the deviation of any field variable from the last iterated value was within 0.01%.

The numerical simulation gives the variation of the field variables in the insulation slab. However, in view of the large number of variables involved, it is useful to identify few parameters to characterize the thermal behavior of the insulation.

The effective thermal conductivity is used to characterize the thermal performance in the presence of condensation and liquid transfer. This is defined as the thermal conductivity of a dry insulation slab which will have a steady heat flux equal to the actual heat flux under the same conditions of temperature. For the equivalent dry slab

$$q_2[1/h + L/k_{\text{eff}}] = T_a - T_2 \quad (27)$$

where q_2 is the heat flux at the cold impermeable surface and k_{eff} is the effective thermal conductivity.

The moisture transfer in the slab is characterized by the moisture gain per unit volume of the insulation slab during a given time. This parameter is obtained by integrating the vapor inflow at the exposed surface over the time interval. The variation of these thermal and moisture flow parameters will be discussed in the next section.

RESULTS AND DISCUSSION

The dynamic response of a porous insulation subjected to the specified boundary conditions has been investigated by case studies. The physical data used are summarized in Table 1. Figures 2(a)–(d) show the variation of the distribution of temperature, vapor density, condensation rate and liquid fraction in the initial phase. As can be seen in Fig. 2(a), when a

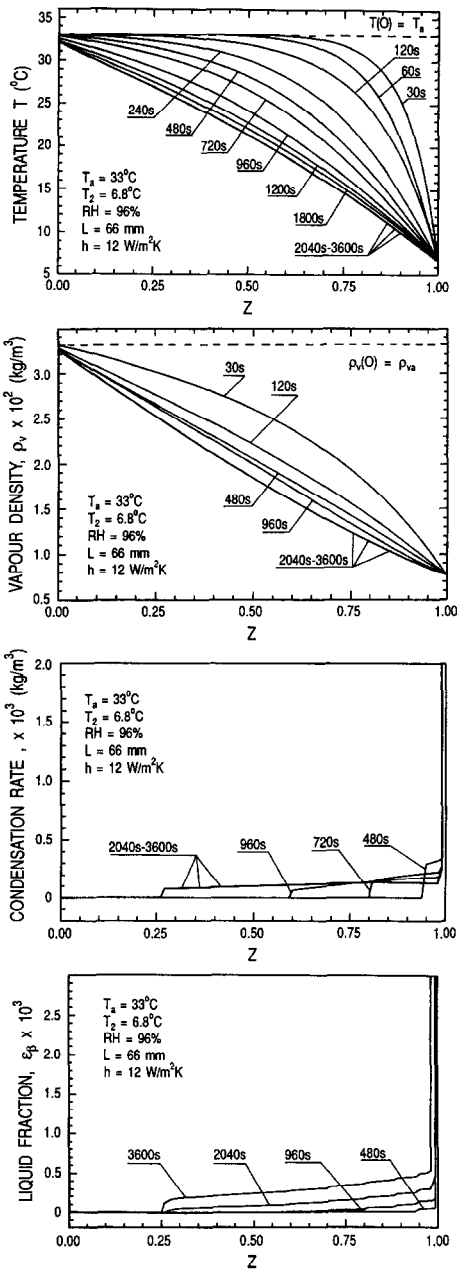

Fig. 2. Distribution of field variables during the initial stage: (a) temperature, (b) vapor density, (c) condensation rate and (d) liquid fraction.

Table 1. Physical data

c_{p0}^* 840 J kg^{-1}K^{-1}	k_0^* 0.037 W m K^{-1}	ρ_0^* 53 kg m^{-3}
$c_{p\sigma}^*$ 836 J kg^{-1}K^{-1}	k_σ^* 0.762 W m K^{-1}	ρ_σ^* 2600 kg m^{-3}
$c_{p\beta}^*$ 4200 J kg^{-1}K^{-1}	k_β^* 0.57 W m K^{-1}	ρ_β^* 999.8 kg m^{-3}
c_{pa}^* 1005 J kg^{-1}K^{-1}	R_a 286.9 J kg^{-1}K^{-1}	ρ_a^* 1.15 kg m^{-3}
c_{pv}^* 1882 J kg^{-1}K^{-1}	R_v 461.9 J kg^{-1}K^{-1}	p_{v0}^* 2337 bar
h_{fg} 2450 kJ kg^{-1}	k_{dry} 0.035 W m K^{-1}	α_{e0}^* 8.31 × 10^{-7} m^2 s^{-1}

porous insulation is suddenly subjected to a temperature drop at the impermeable side, this temperature drop propagates from the cold side into the insulation slab with time. Under the given conditions, the temperature field becomes quasi-steady after about half an hour (2040 s). The propagating behavior is also observed for vapor density as shown in Fig. 2(b), and the vapor density field reaches the quasi-steady state after about the same period. It is apparent that the drop of vapor density propagates faster than that of temperature. It can be expected as the Lewis number is less than one.

The distribution of condensation rate with time is shown in Fig. 2(c). The condensation occurs first at the cold impermeable surface. As the temperature of the slab drops, the location of the condensation front moves towards the warmer side, and stops at some place when the temperature field becomes quasi-steady. The liquid is accumulated with time due to condensation as shown in Fig. 2(d).

The profiles of liquid volumetric fraction over a period of 120 h are shown in Fig. 3. With the establishment of a quasi-steady state, the liquid is accumulated in the wet region at a constant rate. The curve at 1 h indicates that the liquid fraction at the impermeable boundary is higher than the critical value, and liquid diffuses from the cold surface into the insulation slab. From curves between 5 and 60 h, the liquid diffusion front is observed to move towards the dry side of the slab. Before the liquid diffusion front arrives at a point, the liquid accumulates slowly due to condensation. It increases sharply when the liquid front arrives. The liquid front crosses the quasi-steady wet–dry boundary, as indicated by the curve at 70 h, and eventually reaches the exposed surface, as shown by the curves from 80 to 120 h.

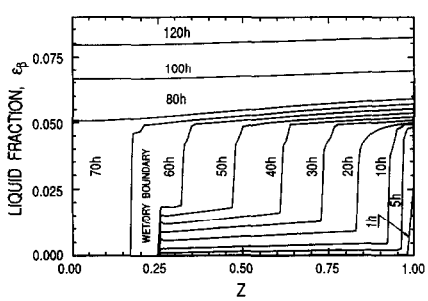

Fig. 3. Liquid fraction distribution over longer period: T_a = 33°C, T_2 = 6.8°C, r.h. = 96%, L = 66 mm and h = 12 W m^{-2} K^{-1}.

Comparison with experimental results

Wijeysundera *et al.* [4] measured the temperature distribution, heat flux, total moisture gain and the liquid distribution for a range of experimental conditions. The testing times were up to 600 h. In the present work, case studies were performed to compare the computational results with the experimental data.

Figure 4(a) shows the temperature distribution in the insulation slab after a quasi-steady state has been established; the numerical results are compared with quasi-steady, constant property analytical results reported in ref. [3]. The experimental results under the same conditions are also plotted in Fig. 4(a), which shows good agreement.

The comparison of computed and measured heat flux and moisture gain for two experimental conditions is shown in Figs. 4(b) and (c). There is good agreement between the computed and measured heat flux for both experimental conditions. The fluctuation of the experimental heat flux is probably due to the slight variations in the experimental conditions [4]. The computed moisture gain shown in Figs. 4(b) and (c) agree well with the measured moisture gain. At longer times the computed moisture gain is slightly larger than the measured value.

The comparison of the computed and measured spatial distribution of the average liquid concentration is shown in Fig. 4(d). There is good agreement between the computed results and measured data for a period of up to about 70 h. The curves for 120 h and 144.5 h show that the predicted rate of liquid movement is faster than the measured. According to measurements the liquid diffusivity becomes significant only when the liquid fraction reaches a very high value of approximately 0.2 for the given conditions. This behavior is different from the experimental observations of Cid and Crausse [18].

A second discrepancy between the measured and computed liquid distribution is related to the variation in the liquid content of the insulation layer with the exposed surface. The experimental data show a rapid rise of the average liquid concentration of that layer after a certain period while the numerical model predicts a far slower growth of the average liquid concentration in the layer. The present model is unable to explain why the layer with the exposed surface has a higher liquid content than the inner layers. A possible explanation is the tendency for the layer with the exposed surface to accumulate liquid due to the surface tension forces between the water and the last

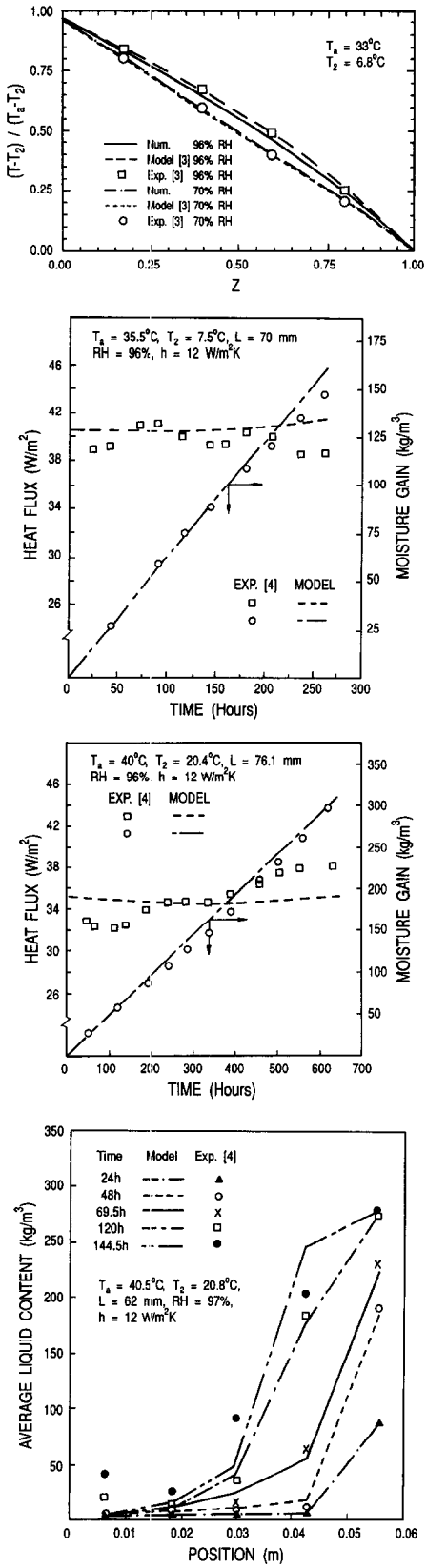

Fig. 4. Comparison of computed results with experimental data [4]: (a) temperature distribution, (b) heat flux and moisture gain, (c) heat flux and moisture gain and (d) average liquid distribution.

layer of fibers on the exposed surface. However, the reason for the liquid to pass through the inner layer without becoming trapped there is not clear.

The liquid transport process is a 2D process with liquid moving along and perpendicular to the direction of the fibers [21, 22]. In the experimental work of Cid and Crausse [18] the liquid diffusion parameters were 'extracted' from infiltration and capillary rise experiments. These processes are somewhat different from the processes occurring in an insulation slab with condensation and liquid transport. Parazak *et al.* [25] have shown that the liquid diffusion parameters cannot be regarded as pure material characteristics because of their strong dependence on initial and/or boundary conditions of the experiment. The differences in experimental conditions could therefore be a reason for the disagreement between the predictions of the liquid transfer model based on the diffusion coefficients in Ref. [18] and the experimental data in ref. [4].

Since the mechanism of moisture movement in fibrous insulation is not completely known, the simulation of the liquid transport process in fibrous materials requires a more rigorous model of liquid transport coefficients.

Thermal performance

The variation of the heat flux at the cold surface as well as the variation of the two components which contribute to the total heat flux, are shown in Fig. 5. In the numerical computation the dependence of the thermal conductivity and the vapor diffusivity on the liquid fraction is taken into account while the analytical model [3] uses constant physical properties at the dry state. The conductive and latent heat flux components show a rapid initial variation due to liquid accumulation at the cold surface. As expected, the conductive component increases while the latent component decreases when more liquid is accumulated, because the presence of liquid in the pore structure increases the effective thermal conductivity but decreases the vapor diffusivity. The net result of the above opposing effects on the total heat flux also

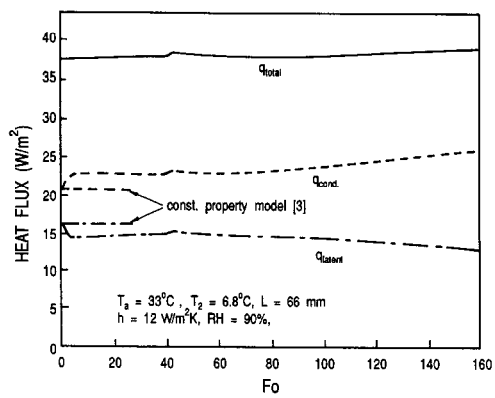

Fig. 5. Variation of heat flux at cold plate with time.

depends on the temperature and humidity conditions to which the insulation is subjected. This is evident from the variations shown in Figs. 4(b) and (c).

A small fluctuation in the heat flux occurs when liquid flows out of the condensation region across the wet–dry boundary as seen in Fig. 5. The increase in the heat flux is a result of the sudden change in the boundary conditions of the system. This causes a change in the temperature gradient at the cold surface which in turn manifests as an increase in the heat flux. The conductive and latent components of the heat flux also display this fluctuation. This fluctuation is too small to be seen in the experimental data shown in Figs. 4(b) and (c).

Parametric study

The variation of the effective thermal conductivity and moisture gain for different design and operating conditions are shown in Figs. 6(a)–(d). It is seen in Fig. 6(a) that increasing the humidity level increases the rate of moisture gain. This leads to a larger total heat flux which in turn gives a larger effective thermal conductivity for the slab. It is also noted that a higher humidity level reduces the time to reach a quasi-steady state. Decreasing the humidity level reduces the length of the condensation region, thus reducing the time for the liquid front to reach the wet-dry boundary.

Figure 6(b) shows the effect of the heat transfer coefficient, h on the variations of $k_{\text{eff}}/k_{\text{dry}}$ and the total moisture gain. It is noted that $k_{\text{eff}}/k_{\text{dry}}$ decreases with increasing h. This behavior can be attributed mainly to the definition of k_{eff}. When h is increased, both the heat flux at the cold plate and the moisture gain increase. As apparent from equation (27), the increased heat flux results in a lower total thermal resistance for the equivalent dry slab. The component $1/h$ of the total thermal resistance decreases as h is increased. The net result of the above two changes is to decrease k_{eff}.

Increasing h decreases the length of the wet condensation region in the slab because of the increase in the temperature of the exposed surface. Also the total moisture gain increases with the increase in h. Due to the above factors, the time taken for the liquid front to reach the wet–dry boundary decreases when h is increased.

The effects of the insulation slab thickness, L on thermal performance and moisture gain are shown in Fig. 6(c). As expected, when slab thickness is decreased, the heat flux at the cold plate and the rate of moisture gain increase. This leads to an increase in k_{eff} as the thickness is decreased. The moisture gain shown in Fig. 6(c) appears to be almost independent of the thickness. This is due to the use of non-dimensional time instead of real time in Fig. 6(c). The total moisture gain varies inversely as slab thickness. Thus the total moisture gain per unit volume of slab varies inversely as the square of the thickness. The nondimensional time Fo also varies as $1/L^2$. The combined effect of the above variations is to make the moisture gain per unit volume almost independent of the slab thickness. Although the real time taken for the liquid front in the slab to reach the wet–dry boundary

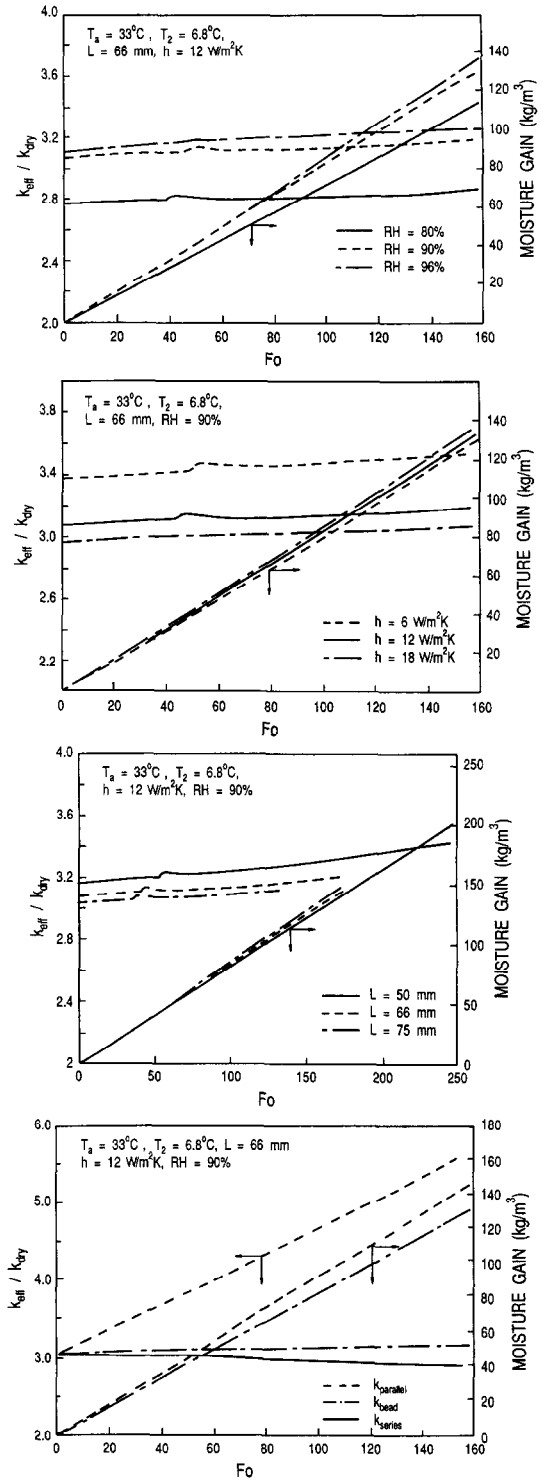

Fig. 6. Variation of $k_{\text{eff}}/k_{\text{dry}}$ and moisture gain for different design and operating conditions: (a) ambient relative humidity, (b) heat transfer coefficient, (c) slab thickness and (d) thermal conductivity model.

increases with slab thickness, the nodimensional time period decreases as seen in Fig. 6(c).

The apparent thermal conductivity of porous insulation in the presence of liquid is greatly dependent on the liquid distribution in the insulation. Reference [19] gives several possible models for thermal conductivity of moisture laden insulations. These models include bead arrangement, series arrangement, parallel arrangement and form arrangement, based on the manner of liquid location in the pores of the insulation.

As shown in Fig. 6(d), the parallel arrangement gives the maximum rates of heat flow and moisture gain. The bead arrangement gives better agreement with the measured heat flux at the cold plate for all runs; it is therefore recommended for computational use. The actual distribution of liquid in the insulation is not completely known. However, the above models give an indication of the sensitivity of the predicted quantities to the variation of the thermal conductivity.

CONCLUSION

A numerical model was developed to study the transient moisture migration through a porous insulation. The predicted liquid distribution, total moisture gain, temperature distribution and heat flux were compared with the experimental data [4]. The effects of intrinsic parameters on thermal performance of porous insulation in the presence of condensation has been investigated.

The following conclusions can be drawn for a typical insulation:

(1) The analysis in the present work has confirmed the four stages of heat and moisture transfer in a porous insulation, which were speculated on the basis of experimental data [4]. The dynamic response and transient behavior with condensation and liquid diffusion are clearly shown. The numerical prediction of quasi-steady behavior has verified analytical results.

(2) The predicted temperature distributions, heat transfer rates and total moisture gains have good agreement with experimental results over various operating conditions for a time period up to 600 h.

(3) The present model used recently measured liquid diffusion coefficients and hydraulic conductivities to predict the liquid distribution in insulations under different conditions. The predictions of the model agrees with experimental data up to about 70 h. For a complete interpretation of liquid distributions, a more accurate liquid transport model and corresponding experimental work is required.

(4) The bead model for thermal conductivity gives good agreement with experimental data for heat flux and moisture gain and could therefore be used in numerical models. The simple model used for the vapor diffusion coefficient also gives good prediction of experimental data.

(5) The effective thermal conductivity of an insulation in the presence of condensation, increases with increasing ambient humidity and decreases with increasing slab thickness and ambient heat transfer coefficient.

(6) The moisture gain per unit volume of insulation increases with increasing ambient humidity and heat transfer coefficient. The rate of moisture gain per unit volume based on nondimensional time is almost independent of slab thickness.

REFERENCES

1. M. K. Kumaran, Moisture transport through glass-fiber insulation in the presence of a thermal gradient, *J. Thermal Insulation* **10,** 243–255 (1987).
2. M. K. Kumaran, Comparison of simultaneous heat and moisture transport through glass-fiber and spray-cellulose insulations, *J. Thermal Insulation* **12,** 6–16 (1988).
3. N. E. Wijeysundera, M. N. A. Hawlader and Y. T. Tan, Water vapor diffusion and condensation in fibrous insulations, *Int. J. Heat Mass Transfer* **32,** 1865–1878 (1989).
4. N. E. Wijeysundera and M. N. A. Hawlader, Effect of condensation and liquid transport on the thermal performance of fibrous insulations, *Int. J. Heat Mass Transfer* **35,** 2605–2616 (1992).
5. D. K. Modi and S. M. Benner, Moisture gain of spray applied insulations and its effect on effective thermal conductivity—I. *J. Thermal Insulation* **8,** 259–277 (1985).
6. S. M. Benner and D. K. Modi, Moisture gain of spray applied insulations and its effect on effective thermal conductivity—II, *J. Thermal Insulation* **9,** 211–223 (1986).
7. C. P. Hedlin, Heat transfer in a wet porous thermal insulation in a flat roof, *J. Thermal Insulation* **11,** 165–188 (1988).
8. Y. Ogniewicz and C. L. Tien, Analysis of condensation in a porous insulation, *Int. J. Heat Mass Transfer* **24,** 421–429 (1981).
9. S. Motakef and M. A. El-Masri, Simultaneous heat and mass transfer with phase change in a porous slab, *Int. J. Heat Mass Transfer* **29,** 1503–1512 (1986).
10. A. P. Shapiro and S. Motakef, Unsteady heat and mass transfer with phase change in porous slab: analytical solutions and experimental results, *Int. J. Heat Mass Transfer* **33,** 163–173 (1990).
11. K. Vafai and S. Whitaker, Simultaneous heat and mass transfer accompanied by phase change in porous insulation, *Trans. ASME, J. Heat Transfer* **108,** 132–140 (1986).
12. K. Vafai and S. Sarkar, Condensation effects in a fibrous insulation, *Trans. ASME, J. Heat Transfer* **108,** 667–675 (1986).
13. K. Vafai and H. C. Tien, A numerical investigation of phase change effects in porous materials, *Int. J. Heat Mass Transfer* **23,** 1261–1277 (1989).
14. H. C. Tien and K. Vafai, A synthesis of infiltration effects on an insulation matrix, *Int. J. Heat Mass Transfer* **33,** 1263–1280 (1990).
15. Y-X Tao, R. W. Besant and K. S. Rezkallah, Unsteady heat and mass transfer with phase changes in an insulation slab: frosting effects, *Int. J. Heat Mass Transfer* **34,** 1593–1603 (1991).
16. S. Whitaker, Simultaneous heat, mass and momentum transfer in porous media: a theory of drying, *Adv. Heat Transfer* **13,** 119–203 (1977).

17. K. Vafai and C. L. Tien, Boundary and inertia effects on flow and heat transfer in porous media, *Int. J. Heat Mass Transfer* **24,** 195–203 (1981).
18. J. Cid and P. Crausse, Influence of the structural characteristics of fibrous heat insulators upon their properties of moisture transfer, *J. Thermal Insulation* **14,** 123–134 (1990).
19. W. J. Batty, P. W. O'Callaghan and S. D. Probert, Apparent thermal conductivity of glass-fiber insulant: effects of compression and moisture content, *Appl. Energy* **9,** 55–76 (1981).
20. D. K. Edwards, D. E. Denny and A. F. Mills, *Transfer Processes*. McGraw-Hill, New York (1976).
21. J. Timusk and L. M. Tenende, Mechanism of drainage and capillary rise in glass-fiber insulation, *J. Thermal Insulation* **11,** 231–241 (1988).
22. S. Motkef and M. A. El-Masri, Liquid diffusion in fibrous insulation, *Trans. ASME, J. Heat Transfer* **107,** 229–306 (1985).
23. S. V. Patankar, *Numerical Heat Transfer and Fluid Flow*. McGraw-Hill, New York (1980).
24. B. F. Zheng, M. Sc. Thesis, University of British Columbia, Canada (1993).
25. J. Prazak, J. Tywonik, F. Peterka and T. Slonc, Description of transport of liquid in porous media, *Int. J. Heat Mass Transfer* **33,** 1105–1120 (1990).